Document downloaded from:

http://hdl.handle.net/10251/58587

This paper must be cited as:

Muñoz Matutano, G.; Rivas, D.; Ricchiuti, AL.; Barrera Vilar, D.; Fernández Pousa, CR.; Martínez Pastor, J.; Seravalli, L.... (2014). Time resolved emission at 1.3 micrometers of a single InAs quantum dot by using a tunable fibre Bragg grating. Nanotechnology. 25(3):35204-1-35204-7. doi:10.1088/09574484/25/3/035204.

The final publication is available at

http://dx.doi.org/10.1088/0957-4484/25/3/035204

Copyright IOP Publishing: Hybrid Open Access

Additional Information

Time resolved emission at 1.3 μm of a single InAs Quantum Dot by using a tunable fibre Bragg grating

G Muñoz-Matutano[1], D Rivas[2], A Ricchiuti[1], D Barrera[1], C R Fernández-Pousa[3], J Martínez-Pastor[2], L Seravalli[4], G Trevisi[4], P Frigeri[4], S Sales[1].

[1] ITEAM Research Institute, Universidad Politécnica de Valencia, C/ Camino de Vera s/n, 46022 Valencia, Spain.

[2]Instituto de Ciencia de los Materiales, Universitat de València, P.O. Box 22085, 46071 Valencia, Spain.

[3]Departamento de Ingeniería de Comunicaciones, Universidad Miguel Hernández, Av. Universidad s/n, E03202 Elche, Spain.

[4]CNR-IMEM Institute, Parco delle Scienze 37a, I-43100 Parma, Italy.

E-mail: Guillermo.Munoz@uv.es

Abstract: Photoluminescence and time resolved photoluminescence from single metamorphic InAs/GaAs quantum dots (QDs) emitting at 1.3 μm have been measured by means of a novel fibre-based characterization set-up. We demonstrate that the use of a wavelength tunable Fibre Bragg Grating (FBG) filter increases the light collection efficiency by more than one order of magnitude as compared to a conventional grating monochromator. We identified single charged exciton and neutral biexciton transitions on the framework of a random population model. The QD recombination dynamics under pulsed excitation can be understood under the weak quantum confinement potential limit and the interaction between carriers at the Wetting Layer (WL) and QD states.

PACS: 68.65.La, 78.66.-w, 71.35.-y, 78.47.jd, 42.79.Ci, 42.81.-i

Introduction:

Single self-assembled semiconductor quantum dots (QDs) are one of the most promising candidates to build versatile photon sources in quantum information technologies [1]. Optical emission from isolated QDs is composed of several spectral lines due to their 0D electronic density of states and the Coulomb interaction between electrons and holes, a behavior that influenced their consideration as artificial atoms. Due to these unique electronic and optical characteristics, In(Ga)As QDs were the basis to develop sources of on-demand single photons and polarization entangled photon pairs [2]. In parallel, progress has been made towards the integation of self-assembled QDs in more complex and refined devices. Some of the breackthroughs have been the increase in the temperature of operation, the emission at longer wavelengths compatible with standard telecommunication technology, and the improvement of the detection efficiencies at these telecom wavelengths.

In this regard, several strategies for improving the operational temperature of SAQDs have been reported, such as the addition of InAlAs barriers during the epitaxial growth of InAs QD to raise the activation energy of the carrier thermal escape [3] or the single photon emission at 45 K with small InP/GaInP QDs [4]. Regarding this important design parameter, there are some growth strategies to obtain QDs samples emitting at the second or third telecommunication windows. The red shift of the InAs/GaAs QD emission by adding additional InGaAs or GaSb capping layers was reported in [5] [6], single QD optical emission at long wavelengths has been reported for InAs QDs grown on metamorphic InGaAs layers [7], [8]. As an alternative to 0D confinement nanostructures it has also been reported the emission from single InAs/InP Quantum Wires (QWRs) at 1.5 μm [9]. Also, it has been proposed a new growth technique to obtain InAs/InP QDs based on the periodic deposition of In and As on InP(001) correlated with surface reconstruction [10], which results in good candidates to design a single photon emitter at 1.5 μm.

Nevertheless, the low detection efficiency and signal to noise ratio of the standard detectors based on InGaAs Avalanche Photodiodes (APD) at long wavelengths (1.0 -1.7 μm) still presents a matter of concern. Careful engineering of the optical loss in the path from source to detector is necessary to maximize the overall detection yield. In addition, the APDs are usually operated under gated mode to increase the signal to noise ratio, a procedure that requires a precise synchronization of the excitation sources, detectors and electronic correlators. In reference [11], for instance, it was demonstrated single photon emission at 1.3 μm of band-pass filtered InAs QD luminescence in a cavity using InGaAs APDs detectors. Here, the whole setup was synchronized by a delay generator triggered through the excitation laser, the APD gate and the Time Correlated Single Photon Counting (TCSPC) board. Using this synchronization procedure

the optical signal under evaluation can be located at the low-noise APD detection window, and precise excitonic and biexcitonic time decays, as well as Hanbury Brown & Twiss (HBT) photon correlation experiments under pulsed excitation measurements could be recorded. However, the repetition rate of the excitation laser under such synchronized detection scheme is limited by the maximum triggering speed of either the delay generator or the APD. Moreover, and although the efforts necessary to synchronize pulsed micro-photoluminescence (μ-PL) experiments are only moderate, synchronized HBT experiments increase the complexity of the set-up because the gate opening of two different APDs must be tuned. The APD gate synchronization was demonstrated as an useful tool in the measurement of the $g^2(0)$ dip in HBT experiments, but this procedure does not give information about the dynamical evolution of the HBT correlation with time delay, $g^2(\tau)$, which is typically extracted from experiments under CW excitation. One of the alternatives to overcome this limitation is to work with expensive cooled superconductor detectors [12], but again at the expense of increasing the complexity of the set-up and also the measurement cost.

In this work we demonstrate a novel instrumentation concept based on a tunable Fibre Bragg Grating (FBG) filter, which permits the time resolved analysis of single quantum dot emission at telecom wavelengths. We fabricated a 1.3-μm band FBG filter with a bandwidth similar to that of conventional grating monochromators, and whose central wavelength can be tuned in a band of more than 4 nm. This mature, low cost, all-fibre technology reduces the typical optical losses of the monochromator filtering more than one order of magnitude. With this technique, conventional InGaAs APD single photon detectors can be used even with no synchronization requirements to manage photons emitted by single QDs. Particularly, we apply this novel method to perform PL and Time Resolved PL (TRPL) spectroscopy on single In(Ga)As QDs emitting at 1.3 μm, which would be hardly measured by using a conventional grating monochromator set-up. In this way, the recombination dynamics of excitons confined in those single QDs can be elucidated given the increased signal-to-noise ratio. Besides the significant reduction in insertion losses, the use of the FBG technology opens the possibility of future integration of single photon emission from FBG-filtered single QDs to standard telecom devices, such as modulators [13], [14], [15] and wavelength routers [16].

Samples and Experimental Set-Up

The metamorphic QD sample under investigation was grown by MBE: after a 100 nm GaAs buffer, a metamorphic $In_{0.15}Ga_{0.85}As$ layer of 500 nm was deposited, followed by 5 nm of GaAs. Then a sub-critical coverage of 1.5 ML of InAs was deposited at 490 °C followed by 20 seconds of annealing under As flux; QDs were capped by 20 nm of $In_{0.15}Ga_{0.85}As$. Single QD emission in

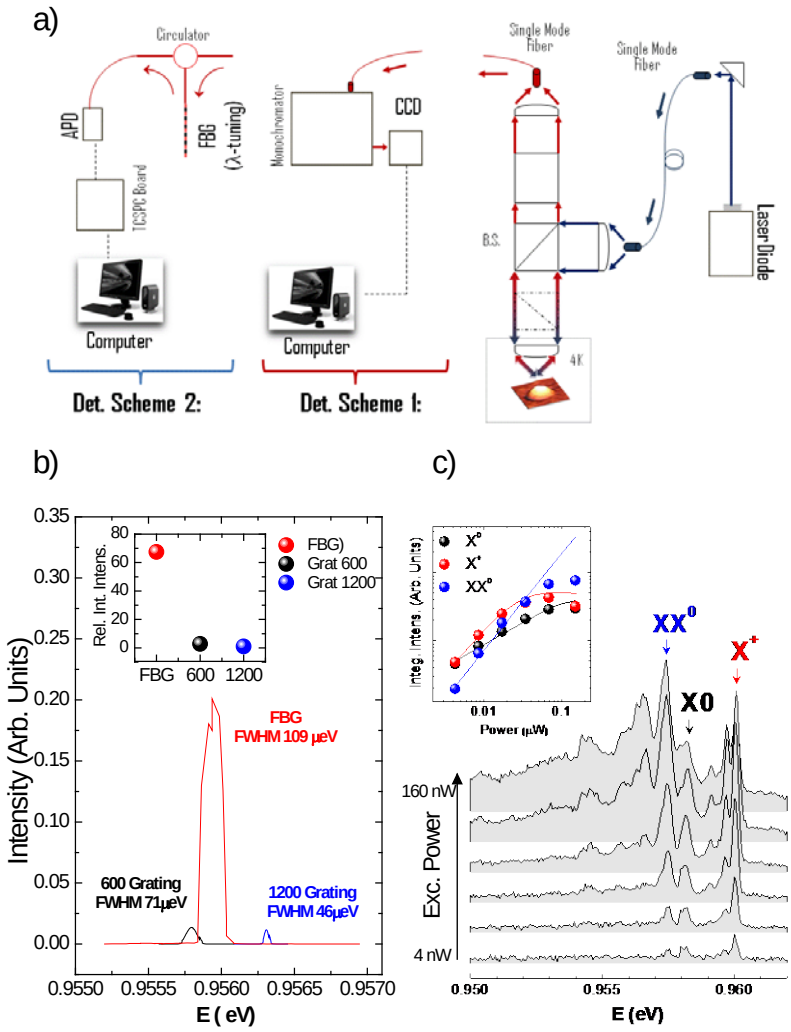

Figure 1: a) Experimental set-up, with two different detection schemes. Detection scheme 1: conventional monochromator and CCD detection. Detection scheme 2: Fibre Bragg Grating filtering. b) FBG and monochromator (with two gratings) efficiency comparison. c) Power dependent µ-Photoluminescence from single QD emitting at 1300 nm. Inset: Integrated Intensity evolution of different excitonic transitions of the QD. Straight lines correspond to the random population model model fitting.

the long wavelength range in these structures has been demonstrated by us in reference [7]. The use of metamorphic InGaAs layer allows for the red-shift of the emission wavelength, thanks to the reduction of strain of QDs and band discontinuities [17], while the deposition of a sub-critical coverage of InAs followed by annealing allows to obtain very low QD density (1 x 10^8 cm^{-2}) for structures grown on metamorphic layers [18].

Figure 1.a shows the experimental set-up. The sample was held in a fibre-based confocal microscope at 4 K to record the single QD optical emission. Positioning of the QD on the excitation/collection spot was carried by three ANP100 Attocube step by step piezo motors, in order to control all x, y and z directions. Two different filtering/detection schemes were implemented. The standard detection scheme 1 is used to obtain conventional μ-PL spectra, exciting the samples with a 790-nm continuous wave (CW) diode laser and analyzing the emission at the collection arm of the confocal microscope through an Andor iDus InGaAs Charged Coupled Device (CCD), attached to a 0.5 m monochromator with two gratings (600 g/mm with 1-μm blaze; 1200 g/mm with 0.75-μm blaze). Detection scheme 2 is used to analyze the QD emission through the FBG filter. The FBG was fabricated using a CW Frequency-doubled Argon ion laser at 244nm and the phase mask technique into a photosensitive optical fibre. The FBG is 3cm long and has an apodization in the modulation of the refractive index that allows reducing the level of the side lobes in the optical spectrum. The central wavelength of the FBG is 1296 nm, with a FWHM of ~ 100 μeV, and a reflectivity of 99.95% of the incident light. After the fabrication, the FBG is placed on a calibrated metal strip in order to tune the central wavelength by compressing or stretching the optical fibre by changing the curvature of the strip. With this procedure we obtained a complete tuning range of more than 4 nm. The signal leaving the tunable FBG is spectrally analyzed by using the same detection scheme described above under CW excitation, in order to reproduce the PL spectrum from a single QD. μ-TRPL was carried under 790 nm pulsed diode laser excitation with 40 MHz repetition rate and FWHM < 70 ps, the reflected light from the FBG is detected by an InGaAs APD (id Quantique single mode id201) attached to a TCSPC board (TCC900 from Edinburgh Instruments), as shown in Figure 1.a (Scheme 2). It was selected the following APD parameters: Internal trigger mode, 1 MHz trigger frequency, dead time of 10 μs and a gate window time of 100 ns. The comparison of optical losses between the monochromator (both gratings) and the FBG device was performed by using a 1300 nm tunable diode laser, having a linewidth lower than 1 MHz, and an optical power meter (Advantest Q8214A).

Results:

Figure 1.b shows the relative amplitude and spectral resolution in the 1.3 μm band of the monochromator for both gratings and the FBG. These traces were obtained by using the 1.3 μm tunable laser at a fixed power of -5dBm, which is subsequently scanned in wavelength and the light intensity recorded with a mono-channel detector. The inset of figure 1.b shows the integrated intensity of the three measured spectra, normalized to the weakest signal (1200 g/mm grating). The FBG filtering produces an optical signal more than 67 times greater than the

filtering made by the 1200 g/mm grating, and 24 times than the filtering made by the 600 g/mm grating. The computation of the relative collection efficiency from the integrated intensity is meaningful when the QD emission linewidth is larger than the FBG or monochromator spectral resolution, as is the case here. In the opposite case of QD linewidths below the spectral resolution, the FBG collection efficiency is about 20 times larger than the monochromator collection efficiency, corresponding to the FBG and monochromator peak intensity ratio. This improvement is a consequence of the absence in the FBG filter of optical losses associated to lens collimation, focalization, multiple reflections and grating efficiency. This is the main reason to use the FBG as a wavelenght selector device for single QD spectroscopy: improving the light collection efficiency to study weak optical signals at 2^{nd} and 3^{rd} telecom windows.

Figure 1.c shows the μ-PL power evolution from an isolated InAs QD, emitting at ~ 1.3 μm as recorded with detector scheme 1. All transitions comes from the same QD emission, as it is demonstrated by the QD scanning through the laser spot from step by step movement of the piezo motors. Optical transitions at 0.9574, 0.9582 and 0.9601 eV are assigned to neutral biexciton (XX^0), neutral exciton (X^0) and positive trion (X^+), respectively. The double logarithmic plot (inset at figure 1.c) shows that X^0, XX^0 and X^+ exhibit potential dependences whose fitted slopes are 0.73, 1.26 and 0.99. The slope deviation from the ideal 1 and 2 for X^0 and XX^0 transitions, and the larger value for X^+ with respect to X^0 can be justified by a random carrier capture mechanism, as previously demonstrated for InAs single QDs emitting at 900-1000 nm [19], [7] In this way, continuous lines at the inset of figure 1.c represent the best fit to the measured integrated intensity variation by using a random population model [19]. The good agreement demonstrates the validity of the above given excitonic assignation, except for the case of XX^0 intensity at high excitation powers, because we only considered S levels for the QD. We measured a binding energy of 0.8 meV for XX^0, which is slightly lower than similar results on QDs grown by MOCVD [20], [21], and MBE [7], emitting at a similar wavelength. The μ-PL linewidth was considerably reduced (~ 250 μeV) compared to previous samples (1 meV in reference [7]).

The maximum recorded signal intensity was around 100 counts/s for the XX^0 transition under CW excitation (figure 1.c), by using the detector scheme 1. However, the optical signal decreases to extremely low levels with the InGaAs CCD under pulsed operation and integration times of 10-60 seconds. This is a common single QD emission feature, which is related to the instantaneously high-density carrier feeding under laser pulse absorption [22], [23]. Therefore, μ-PL transients using gated InGaAs APDs are hardly measured, as the QD optical signal is much lower than the noise level. The use of the enhanced FBG detection technique (detection scheme 2 in fig 1.a) offers a great advantage for this purpose, because it is neither required

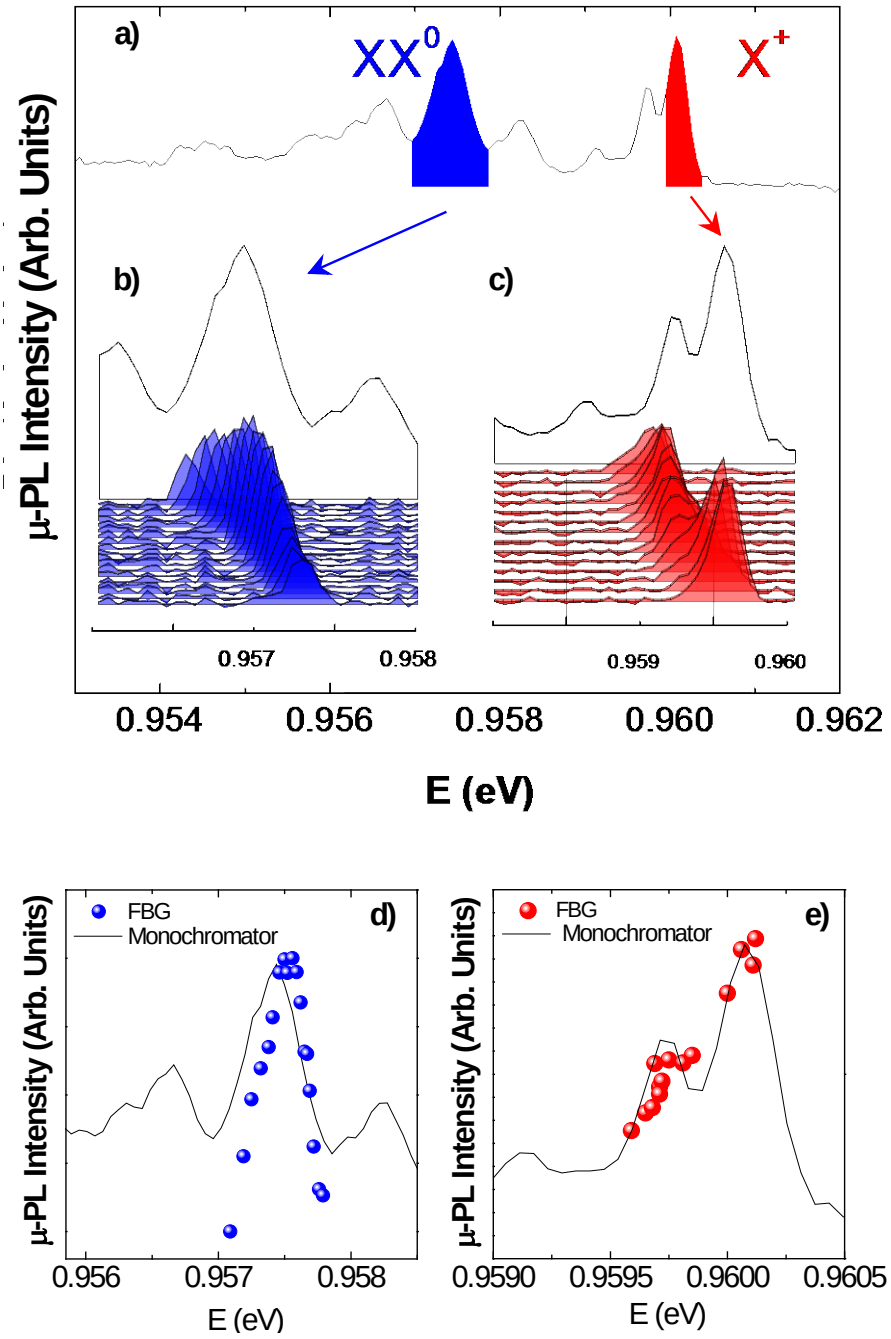

Figure 2: a) μ-Photoluminescence spectrum recorded with detection scheme 1 at excitation power of 81 nW. b) and c) Fibre Bragg Grating tunning (color) of XX^0 (blue) and X^+ (red) transitions, respectively, compared with the spectrum from a) (black line). d) and e) Integrated Intensity versus peak position of each acquisition at b) (blue dots) and c) (red dots), respectively, compared to the spectrum in a).

sophisticated and costly detection systems nor a synchronized set-up. In this way the intrinsic

spontaneous emission of single QDs can be analyzed without embedding them in engineered photonic cavities, in which spontaneous emission is altered by the Purcell effect.

Figure 2 shows the comparison between the QD spectrum in figure 1.c (excitation power = 160 nW) and the light analyzed with the FBG technique. The wavelength tuning range covers both X^+ (red) and XX^0 (blue) transitions (ΔE = 3.2 meV, $\Delta\lambda$ = 4.4 nm), as observed in figure 2.a. Figures 2.b and 2.c show the comparison between the spectra of the X^+ and XX^0 transitions from figure 1.c and the FBG spectra with wavelength tuning (figure 2.a and 2.b). Figures 2.d and 2.e show the FBG based reconstructed spectra by plotting the integrated intensity of FBG spectra versus their peak energy, as extracted from figures 2.b and 2.c. The FBG filtering spectra perfectly matches those registered by the CCD-Spectrograph, which demonstrates that the present method is equivalent to a mono-channel detection system.

As aforementioned, the tunable FBG filtering method is the only detection set-up able to measure μ-TRPL spectra of single QD optical transitions in our sample with standard InGaAs APDs, as shown in figure 3.a and 3.b for X^+ and XX^0 transitions, respectively. Here we describe the results found in the TRPL analysis. A clear increase of the rise time is observed by increasing the excitation power, simultaneously to the appearance of a time delay between a fast decay contribution and the slow μ-TRPL transient of the corresponding exciton especies. This is a result from different time phases of the QD recombination after the absorption of the excitation pulse [24]. The fast transient has been reported in literature and explained by the recombination of a broad emission, which is related to the many body Coulomb interaction at the QD after the absorption of high intensity pulses [24], [23]. In order to extract the time constants and to simulate the fast and slow μ-TRPL components, we used the following time dependent expression of the QD intensity:

$$I(t) = I_0 + \frac{1}{w}\sqrt{\frac{\pi}{2}}e^{-\frac{2t^2}{w^2}} * \left[I_{fast}F_{w_F}(t-t_0) + I_{Slow}\left(e^{-\frac{(t-(t_0+D))}{\tau_d}} - e^{-\frac{(t-(t_0+D))}{\tau_r}}\right)H\big(t-(t_0+D)\big)\right] \quad (1)$$

The first term (I_0) corresponds to the presence of a TRPL flat background (time uncorrelated noise). The second term is the convolution of the system APD response (Gaussian with w = 0.38 ns) with the TRPL decay term (* means convolution). This decay term is divided by fast and slow components. The fast decay is limited by the temporal response of our system, and can

be also simulated by a Gaussian profile $\left(F_{w_F}(t-t_0) = \frac{1}{w_F}\sqrt{\frac{\pi}{2}}e^{-\frac{2(t-t_0)^2}{w_F^2}}\right)$, with w_F = 0.2 ns. The last term in equation 1 represents the slow decay component. It is composed by rise and decay exponentials, characterized by their corresponding times constants τ_r (rise time) and τ_d

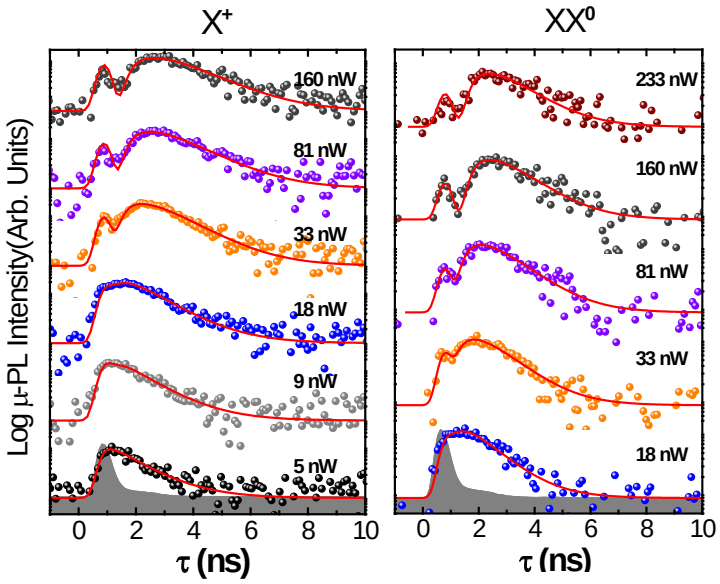

Figure 3: Power dependent μ-Time Resolved Photoluminescence evolution from X^+ (left panel) and XX^0 (right panel) QD optical transitions. In both panels, grey shadow corresponds to the system response. With straight red lines are represented the best fittings of the experimental decays with the equation described in the text.

(decay time). D is the delay time of the slow decay with respect to t_0 (time of the maximum intensity associated to the fast decay). Finally, this last term is multiplied by the Heaviside function, which is zero for $t < t_0 + D$. It is important to notice that we fitted all TRPL transients with fast and slow decay components for all the excitation powers (continuous red lines in figures 3.a and 3.b).

Discussion

Following the μ-TRPL fitting described in the previous section we analyzed the excitonic and biexcitonic decay time (τ_d), rise times (τ_r) and delay time (D) values along the excitation power range. τ_d of X^+ and XX^0 are constant in the whole power range with values of 1.15 and 0.96 ns, respectively. On the contrary, we find τ_r and D to be power dependent (figures 4.a and 4.b). Figure 4.b shows that τ_r of X^+ increases from hundreds of ps to near 1 ns at high excitation

power. This value is very close to the XX^0 decay time (0.96 ns), whereas the rise time for XX^0 grows from ~ 0.4 ns to a maximum value of 0.7 ns. The difference between τ_r of X^+ and XX^0 asymptotic values can be understood by the quantum cascade of photons between biexcitons and excitons [25], [26]. The X^+ excitonic specie can be created after the neutral biexciton recombination and a single hole capture, after the recombination of the positively charged biexciton (XX^+) and its carrier relaxation, or other similar multiexciton recombination processes. In all of these possibilities we would expect larger rise times for X^+ TRPL than for XX^0 TRPL, as the single exciton recombination must occur after the biexcitonic transition. On the other hand, the XX^0 transition must wait for higher order multiparticle recombinations events, which are expected to be characterized by shorter decay times.

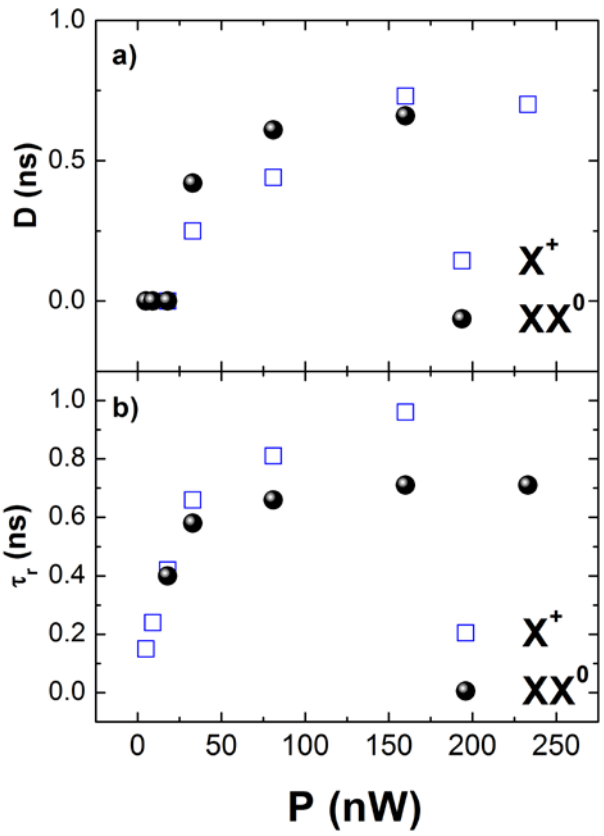

Figure 4: a) Delay time (D) evolution with the excitation power for X^+ (open squares) and XX^0 (filled spheres) transitions. b) Rise time (τ_r) evolution with the excitation power for X^+ (open squares) and XX^0 (filled spheres) transitions.

The delay time of the slow decay component (D) also shows an increase with the excitation power. However, in this case no significant differences between the X^+ and XX^0 delay time evolution are observed (Figure 4.a). We tentatively propose that this delay time would be associated to the fast relaxation of the high density carrier feeding to the WL after the laser pulse absorption at the GaAs barrier. As the laser pulse is more intense, the number of carriers absorbed within the laser spot increases substantially, and the time needed to dilute the WL carrier density grows accordingly. We associate the physical origin of this delay time and the fast decay recombination process with the interaction of this high density of carriers at the WL, spatially localized at the excitation spot (diameter ~ 1 μm), with the carriers being trapped at the QD levels. It has been shown previously how the carriers at the QD would interact with a filled continuum producing a spectral broadening of the excitonic transitions [27]. Furthermore, WL-QD carrier interaction was proposed before to explain the origin of the broad spectrum at the QD emission energy [28]. Here, we show that the delay time D between fast and slow decays could be considered as one fingerprint of the WL-QD carrier interaction.

Finally, the existence of a similar decay time for XX^0 and X^+ transitions could be understood in the framework of the weak quantum confinement potential limit. Radiative recombination rates are strongly affected by the quantum correlation of electrons and holes [29]. For the strong quantum confinement regime it is expected a ratio $\tau_d^{X^0}/\tau_d^{XX} = 2$. Also, $\tau_d^{X^+} \cong \tau_d^{X^0}$ and hence in this limit $\tau_d^{X^+}/\tau_d^{XX} \cong 2$. On the other hand, and due to the Coulomb interaction between carriers, in the weak quantum confinement limit it was found $\tau_d^{X^0}/\tau_d^{XX} < 1$ [30] [31] and some differences between the X^0 and X^+ decay times are expected, even with $\tau_d^{X^+}$ significantly larger than $\tau_d^{X^0}$ [32]. In our case we have found $\tau_d^{X^+}/\tau_d^{XX} = 1{,}2$. InAs bulk Bohr radius (a_B) is 25 nm, and in these samples with $In_{0.15}Ga_{0.85}As$ metamorphic layers the diameter of QD (d_{QD}) can be estimated to be in the 30-45 nm range [18], which is larger than the sizes of metamorphic QDs grown with the SK method [33], [34]. The ratio $d_{QD}/a_B > 1$ justifies the weak quantum confinement limit, where a deviation from the strong confinement time decay relation ($\tau_d^{X^+}/\tau_d^{XX} = 2$) is hence expected.

Conclusion

In conclusion, we have proposed a novel μ-PL characterization technique of QDs based on the light filtering through a wavelength tunable FBG. This wavelength tuning capability, together with the increased light collection efficiency of the FBG, offer a great advantage to study μ-TRPL of the different excitonic transitions, by using conventional InGaAs APD detectors. Along with these operational improvements, the wavelength tunable FBG offers an easy and

cheap alternative characterization tool, which could be easily integrated to more complex signal treatments, as phase or amplitude modulators. With the help of our set-up improvement, we studied μ-TRPL from single QD optical transitions at 1.3 μm at low temperatures and elucidated their recombination dynamics. Time decays from biexciton and positive trion optical transitions are understood by assuming a weak quantum confinement QD potential, which is in concordance with the QD size. We have also found evidences of a fast TRPL dynamics associated to the interaction between carriers at the WL and QD states. In future applications, the increase of collection efficiency with FBG filtering should result in a higher SNR ratio in HBT experiments, thus permitting a more precise characterization of the $g^2(0)$ value. At the same time the FBG spectral filtering method applied to the XX^0- X^0 cascade emission could be used to force the entanglement [35], and hence to demonstrate that our QDs can be used as a single photon emitters, or sources for polarization photon entanglement, at the second telecom window. Furthermore, the photon collection by the FBG would be a simple way to build such sources for quantum information management.

Acknowledgements

G. Muñoz-Matutano would like to appreciate the valuable help from Professor Miguel Andrés (University of Valencia) and thanks the Spanish Juan de la Cierva program (JCI-2011-10686). We acknowledge the support of the FEDER actions UPVOV08-3E-008 and UPVOV10-3E-492, the PROMETEO2009/74 project from Generalitat Valenciana, the Spanish projects TEC2011-29120-C05-01-02-05, the support of the Italian FIRB Project "Nanotecnologie e Nanodispositivi per la Società dell'Informazione" and by the "SANDiE" Network of Excellence of EC, Contract No. NMP4-CT-2004-500101.

References

[1] D. Bimberg, Ed., Semiconductor Nanostructures, Berlin Heidelberg: Springer-Verlag , 2008.

[2] C Salter, R Stevenson, I Farrer, C Nicoll, D Ritchie and A Shields 2010 *Nature* **465** 594

[3] L Seravalli, G Trevisi, P Frigeri, S Franchi, M Geddo and G Guizzetti 2009 *Nanotechnology* **20** 275703

[4] A K Nowak, E Gallardo, D Sarkar, H P v d Meulen, J M Calleja, J M Ripalda, L González and Y González 2009 *Phys Rev B* **80** 161305(R)

[5] G Trevisi, L Seravalli, P Frigeri and S Franchi 2009 *Nanotechnology* **20** 415607

[6] J M Ripalda, D Alonso-Álvarez, B Alén, A G Taboada, J M García, Y González and L González 2007 *Appl. Phys. Lett.* **91** 012111

[7] L Seravalli, G Trevisi, P Frigeri, D Rivas, G Muñoz-Matutano, I Suárez, B Alén and J Martínez-Pastor 2011 *Appl. Phys. Lett.* ***98*** 173112

[8] E Semenova, R Hostein, G Patriarche, O Mauguin, L Largeau, I Robert-Philip, A Beveratos and A Lemaitre 2008 *J. Appl. Phys.* **103** 103533

[9] B Alén, D Fuster, Y González, L González and J Martínez-Pastor 2006 *Appl. Phys. Lett.* **89** 233126

[10] D Fuster, A Rivera, B Alén, P Alonso-González, Y González and L González 2009 *Appl. Phys. Letts* **94** 133106

[11] C Zinoni, B Alloing, C Monat, V Zwiller, L H Li, A Fiore, L Lunghi, A Gerardino, H d Riedmatten, H Zbinden and N Gisin 2006 *Appl. Phys. Lett.* **88** 131102

[12] R Hadfield 2009 *Nature Photonics* **3** 696

[13] J Capmany and C R Fernandez-Pousa 2010 *J. Opt. Soc. Amer. B* **27** A119

[14] S Ates, I Agha, A Gulinatti, I Rech, A Badolato and K Srinivasan 2013 *Scientific Reports* **3** 1397

[15] M T Rakher and K Srinivasan 2011 *Appl. Phys. Lett.* **98** 211103

[16] J Capmany, J Mora, C Fernández-Pousa and P Muñoz 2013 *Optics Express* **21** 14841

[17] L Seravalli, M Minelli, P Frigeri, S Franchi, G Guizzetti, M Patrini, T Ciabattoni and M Geddo 2007 *J. Appl. Phys.* **101** 024313

[18] L Seravalli, G Trevisi and P Frigeri 2012 *Crys. Eng. Comm.* **14** 6833

[19] J Gómis-Bresco, G Muñoz-Matutano, J Martínez-Pastor, B Alén, L Seravalli, P Frigeri, G Trevisi and S Franchi 2011 *New Journal of Phys.* **13** 023022

[20] A Fiore, C Zinoni, B Alloing, C Monat, L Balet, L Li, N L Thomas, R Houdre, L Lunghi, M Francardi, A Gerardino and G Patriarche 2007 *J. of Phys: Cond. Matter* **19** 225005

[21] N I Cade, H Gotoh, H Kamada, T Tawara, T Sogawa, H Nakano and H Okamoto 2005 *Appl. Phys. Lett.* **87** 172101

[22] T Kuroda, S Sanguinetti, M Gurioli, K Watanabe, F Minami and N Koguchi 2002 *Phys. Rev. B* **66** 121302(R)

[23] L Landin, M S Miller, M E Pistol, C E Pryor and L Samuelson 1998 *Science* **280** 262

[24] C Zinoni, B Alloing, C Monat, L H Li, L Lunghi, A Gerardino and A Fiore 2006 *Phys Stat Sol (c)* **11** 3717

[25] E Moreau, I Robert, L Manin, V Thierry-Mieg, J M Gérard and I Abram 2001 *Phys. Rev. Lett.* **87** 183601

[26] E Dekel, D V Regelman, D Gershoni, E Ehrenfreund, W V Schoenfeld and P M Petroff 2000 *Phys Rev B* **62** 11038

[27] P A Dalgarno, M Ediger, B D Gerardot, J M Smith, S Seidl, M Kroner, K Karrai, P M Petroff, A O Govorov and R J Warburton 2008 *Phys. Rev. Lett.* ***100*** 176801

[28] N Chauvin, C Zinoni, M Francardi, A Gerardino, L Balet, B Alloing, L H Li and A Fiore 2009 *Phys Rev B* **80** 241306

[29] G Bacher, R Weigand, J Seufert, V D Kulakovskii, N A Gippius, A Forchel, K Leonardi and D Hommel 1999 *Phys. Rev. Lett.* **83** 4417

[30] S Kono, A Kirihara, A Tomita, K Nakamura, J Fujikata, K Ohashi, H Saito and K Nishi 2005 *Phys. Rev. B* **72** 155307

[31] M Wimmer, S V Nair and J Shumway 2006 *Phys. Rev. B* **73** 165305

[32] P A Dalgarno, J M Smith, J McFarlane, B D Gerardot, K Karrai, A Badolato, P M Petroff and R J Warburton 2008 *Phys. Rev. B* ***77*** 245311

[33] L Seravalli, P Frigeri, L Nasi, G Trevisi and C Bocchi 2010 *J. Appl. Phys.* **108** 064324

[34] L Seravalli, M Minelli, P Frigeri, P Allegri, V Avanzini and S Franchi 2003 *Appl. Phys. Lett.* **82** 2341

[35] Y Kodriano, E Poem, N H Lindner, C Tradonsky, B D Gerardot, P M Petroff, J E Avron and D Gershoni 2010 *Phys. Rev. B* **82** 155329